Nanoscale

Accepted Manuscript

This article can be cited before page numbers have been issued, to do this please use: G. Laucirica, V. Cayón, Y. Toum Terrones, M. L. Cortez, M. E. Toimil-Molares, C. Trautmann, W. A. Marmisollé and O. Azzaroni, *Nanoscale*, 2020, DOI: 10.1039/C9NR10336H.

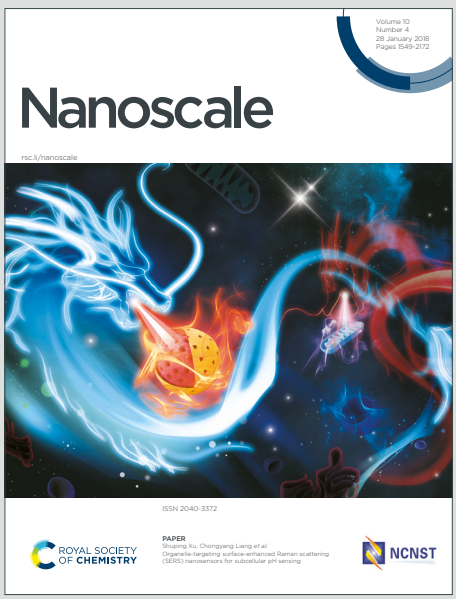

ROYAL SOCIETY OF CHEMISTRY

rsc.li/nanoscale

Electrochemically addressable nanofluidic devices based on PET nanochannels modified with electropolymerized poly-*o*-aminophenol films

View Article Online
DOI: 10.1039/C9NR10336H

Gregorio Laucirica,[1] Vanina M. Cayón,[1] Yamili Toum Terrones,[1] M. Lorena Cortez,[1] María Eugenia Toimil-Molares,[2] Christina Trutmann,[2,3] Waldemar A. Marmisollé[1,*] and Omar Azzaroni[1,*]

[1]Instituto de Investigaciones Fisicoquímicas Teóricas y Aplicadas (INIFTA), Departamento de Química, Facultad de Ciencias Exactas, Universidad Nacional de La Plata, CONICET – CC 16 Suc. 4, 1900 La Plata, Argentina

[2]GSI Helmholtzzentrum für Schwerionenforschung, 64291 Darmstadt, Germany

[3]Technische Universität Darmstadt, Materialwissenschaft, 64287 Darmstadt, Germany

Abstract

Nanofluidic field-effect transistors (nFETs) have attracted the attention of scientific community due to its remarkable level of control over ionic transport. Particularly, the combination of nanofluidic systems and electroactive polymers has demonstrated being an interesting approach to achieve an electrochemically addressable device. In this work, the development of nFETs based on the integration of electropolymerized poly-o-aminophenol (POAP) films into track-etched nanochannels is proposed. The electropolymerization of POAP on the tip side of Au-sputtered asymmetric PET nanochannels allowed not only having a programmable tip diameter but also offered precise and very rapid control of ionic transport by switching an external bias voltage. Moreover, the system exhibited a reversible behaviour between non-selective and anion-selective states. We believe that this work provides new tools and concepts to design and build high-performance nanofluidic field-effect transistors working under electrochemically controlled conditions.

Introduction

Biological ionic channels are transmembrane proteins that allow ionic flux between a cell and its external medium.[1] Up to now, a wide variety of ionic channels with different features is known. Despite the broad spectrum of biological channels, most of them have some common important properties as, for example, ionic selectivity and stimulus-responsiveness.[2] Thereby, channels able to trigger a response (*i.e.*: signal) in presence of a certain stimulus as, for example, an external electric field or changes in some ligand concentrations, endow the channel with the desirable feature of stimulus-responsiveness. The fascinating properties of biological ionic channels have inspired the design of abiotic nanopores (solid-state nanochannels, SSNs) using materials that

* E-mail: azzaroni@inifta.unlp.edu.ar (O.A.)
E-mail: wmarmi@inifta.unlp.edu.ar (W.A.M.)

View Article Online
DOI: 10.1039/C9NR10336H

provide versatility, robustness and resistance to different environmental conditions together with a precise ionic flux control.[3–6]

Particularly, the development of SSNs in polymer membranes by the ion-track-etching technique has attracted special attention due to several reasons.[7] Firstly, the channel surface obtained by this technique exhibits carboxylate groups that produce, at suitable conditions, charged surfaces allowing both its operation as an ionic filter and subsequent surface modifications.[8,9] Moreover, this method allows the development of nanochannels with tailored geometries.[10–13] The rupture of electrical potential introduced by asymmetric shapes is crucial as it leads to the development of devices with ionic current rectification (ICR).[14] The ICR implies that the current is favoured in a certain polarity of transmembrane voltage over the reverse polarity, *i.e.* there is a diode-like charge transport. This phenomenon has been used in several applications such as biosensing, the development of ionic diodes and ionic filters, among others.[9,15–17] Alternatively, asymmetric current flows can be also achieved by asymmetric surface modifications and even by heterogeneous surface charge distributions.[18]

To imitate the biological counterpart, researchers have shown great interest in the development of devices with ionic fluxes that are subjected to external and non-invasive stimuli. In this sense, SSNs responsive to a wide variety of stimulus such as light, temperature, pH and chemical effectors have been designed.[19–22] In this regard, the application of a bias voltage as a non-invasive effector in order to control the ionic flux through the SSN emerges as an interesting option.[23] Given the similarities between these systems and the field-effect transistor (FET), these devices can be referred to as nanofluidic field-effect transistors (nFETs) and the bias voltage can be considered as the gate voltage (V_g) in traditional FETs.

In the last years, researchers have attained to control ionic transport by means of V_g using different strategies. Within the field of two-dimensional nanofluidic devices, in the last years voltage-gated responses have been achieved by a variety of configurations and materials,[24] such as graphene[25,26] and graphene oxide stacks membranes[27] and more recently by the laminar assembly of Mxenes.[28] Concerning ionic transport through nanochannels in polymer membranes, seminal works of Martin *et al.* in Au nanotubules membranes showed that the application of a V_g allows controlling the Au surface charge excess and this fact produces a direct effect on the ionic transport of ions through the nanotubule.[29] At the beginning, the voltage-gated transport in track-etched membranes was achieved by means of successive deposition of semiconductor and metal layers onto polymer foils.[30] Recently, a new generation of nFETs was introduced, where the successive semiconductor depositions were replaced by the controlled growing of electroactive polymer layers.[31–33] Added to the ease of preparation, these systems opened the floodgates to the design of a wide variety of arrays by exploiting the interesting attributes of electroactive polymers.[34–36] Nevertheless, despite the advantages exhibited by nFETs based on electroactive polymers, their study remains scarce. In this context, it is necessary to continue exploring the rational design and synthesis of nFETs devices that meet favourable features such as robustness, reproducibility, and quick response, among others.

Electroactive polymers are polymers that can be reversibly oxidized or reduced by means of, for example, the application of a bias voltage.[37,38] Moreover, taking into account its electron-transport mode, these polymers can be classified into two groups: electronically conducting polymers (CPs) and redox polymers (RPs). On one side, RPs contain redox sites electrostatically or covalently attached to the polymer structure, such as in

the case of poly-(vinylferrocene) and quinone-polymers. The electron transport in these systems is carried out by electron hopping. On the other hand, CPs structure is constituted by double bound conjugated chains, which allows the charge conduction along the polymer. Among the whole family of CPs, polypyrrole (PPy), poly(3,4-ethylenedioxothiophene) (PEDOT) and polyaniline (PANI) are the most archetypal examples. Within this last group, PANI has been one of the most studied polymers. The robustness and chemical stability of PANI has positioned it as a good candidate for the development of biosensors, supercapacitors, electrochromic devices, and batteries, among other applications.[39–42] The extraordinary properties of PANI encouraged researchers to synthesize polymers based on substituted anilines such as poly-(*o*-aminophenol) (POAP).[43,44] POAP is a widely studied polymer synthesized from *ortho*-aminophenol (*o*-AP).[45–47] However, unlike aniline, *o*-AP polymerization renders a redox-type polymer, with two redox states (**Figure 1**). Moreover, the chemical nature of quinone redox couples confers the POAP films a high permselectivity.[48,49] These characteristics turn POAP into a good candidate for the development of smart SSN-based platforms with voltage-gated selectivity.

In this work, we present the development of a voltage-gated nanofluidic diode based on the electrochemical polymerization of *o*-AP in asymmetric gold-coated polyethylene terephthalate (PET) single nanochannels. Particularly, we show that the site-selective electrosynthesis of POAP at the small opening (*i.e.*: the tip) of the nanochannel confers properties of ionic current rectification to the nanofluidic device. We found that external gate voltages applied to the device can be used to control the redox state of the polymer in the nanochannel and, consequently, to dictate its ion transport and current rectification properties. We believe that the reversible redox characteristics offered by POAP films in combination with the remarkable physical characteristics of asymmetric nanopores constitute a new framework for the design of multifunctional nanofluidic devices employing external voltages as non-invasive stimulus to trigger a predefined iontronic response.

Results and discussion

First, bullet-shaped single nanochannels in PET foils (12 μm thickness) were fabricated by the ion-track-etching method.[7] For this purpose, the foils were irradiated with a single swift heavy ion and subsequently exposed to a chemical etchant. Thus, asymmetric bullet channels were obtained by surfactant-assisted etching.[50] Then, the foils were coated with a gold layer (~80 nm) on the tip side via sputtering. This method led to nanochannels with small openings diameters (d_{tip}) of ~80 nm and base diameters (D) of ~650 nm (**Figure S1**). The Au-coated side on the membranes was then modified with a POAP layer by electropolymerization.

As reported by Tucceri, *ortho*-amino-phenol (*o*-AP) can be polymerized electrochemically in acidic, neutral and alkaline solutions.[46]. However, whereas an electroactive film is formed in acidic media, POAP films synthesized in neutral and alkaline media present no electroactivity.[46] Therefore, the metallized foils were modified by *in situ* electropolymerization of *o*-AP according to the experimental conditions described by Barbero *et al*.[51] The electrosynthesis was carried out by cyclic voltammetry in acidic medium (2 mM *o*-AP in 0.1 M $HClO_4$ / 0.4 M $NaClO_4$, pH~1) using a classical three-electrode array in which the gold-sputtered membrane was used as working electrode. The metallized membrane was subjected to subsequent potential scans (**see SI file**) for depositing a film of the electroactive polymer onto the side of the nanochannel tip.

The mechanism of electro-oxidation of *o*-AP involves different chemical steps (**Figure 1(a)**).[51] In **Figure 1 (b)**, voltammograms for the synthesis of POAP at different stages (*i.e.*: number of voltammetric cycles) of the electropolymerization are shown. On the first positive sweep, a broad peak, ***a,*** can be noticed in the region 0.7-0.75 V due to the oxidation of *o*-AP to monocation radical (*o*-AP•$^{+}$) and then to dication radical (o-AP•$^{2+}$). On the negative sweep, this broad peak does not show a complementary one, indicating chemical follow-up reactions giving products detected as peaks ***b-b'*** and ***c-c'*** on the subsequent sweeps. The peak system ***c-c'*** increases on cycling, showing the characteristic behaviour of a deposited electroactive substance, *i.e.* the formation of the POAP film.[46] The overall polymer formation reaction is depicted in **Figure 1 (a)**.

Cyclic voltammetry results of the POAP film deposited into the tip side of the nanochannel are shown in **Figure 1(c)**. Thereby, these voltammograms reveal the redox switching of POAP (**Figure 1 (a))** in acidic media that arises from the deposited electroactive POAP film. Unlike other electroactive polymers based on substituted aniline, the voltammetric wave is characterized for only one redox reaction placed at bias voltages of ~0-0.1 V vs Ag/AgCl.[21,44] Specifically, the redox couple is centred at ~65 mV at pH=1 which is in good agreement with previously reported values.[46,51] Furthermore, a POAP film thickness of ~25-30 nm could be estimated by the voltammetric charge that comes from the reduction peak (see Reference [43] for further details).

The voltammogram in **Figure 1 (c)** is not symmetric, suggesting a complex redox behaviour that does not follow the simple Nernstian model (further details about the electrochemical behaviour of POAP are available in the SI file, **Figure S2**).[46] Previous studies have demonstrated that variables, such as film thickness, solution pH and redox couple concentrations in solution affect both the permeation process of electroactive species and the electron motion through a POAP film.[52–54]

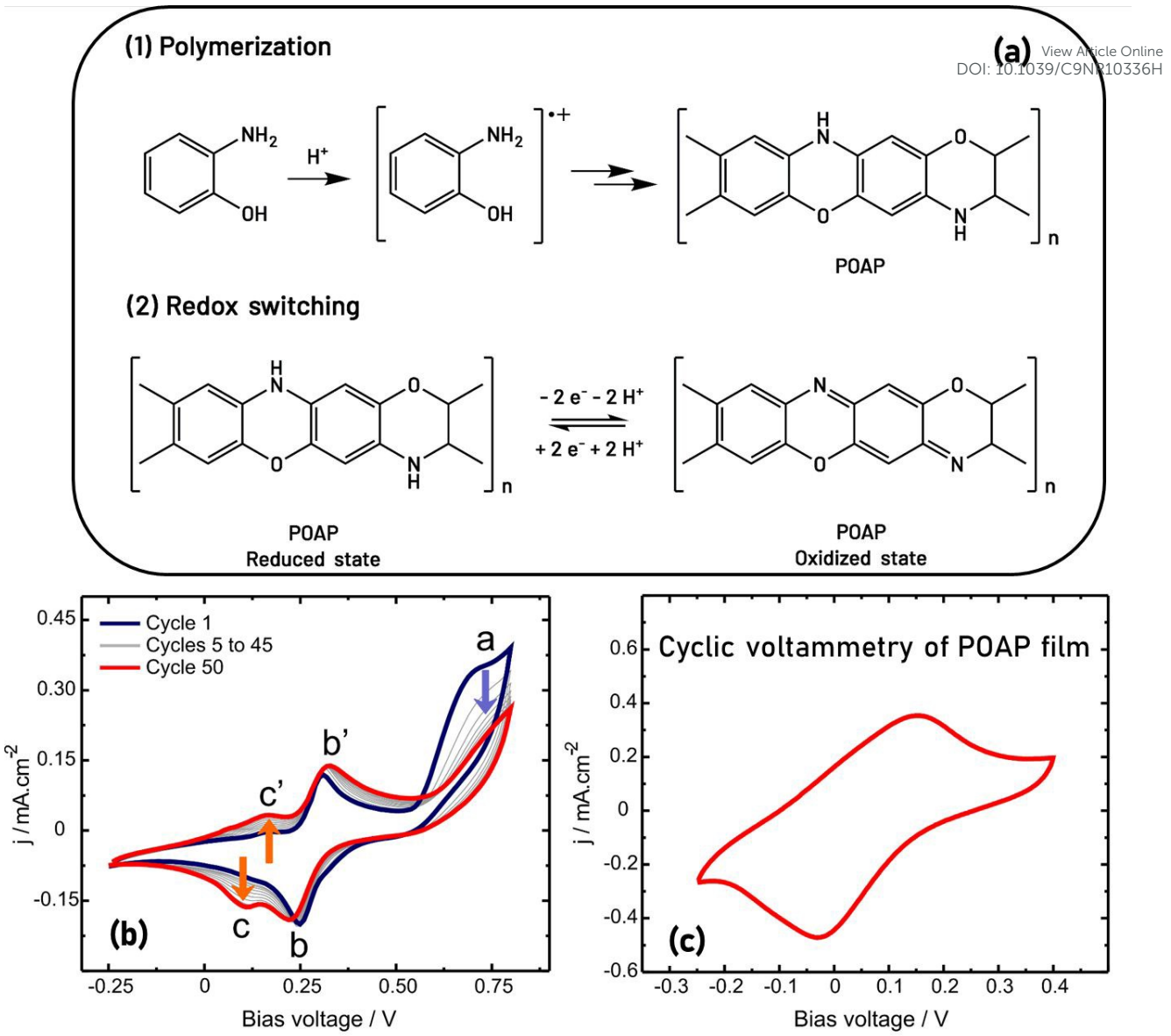

Figure 1. **(a)** Reaction schemes: (1) POAP formation reaction from *o*-AP and (2) POAP redox switching; **(b)** Voltammograms for the synthesis of POAP at different steps of the electropolymerization: at the beginning (blue, 1st cycle), between 5th and 45th cycles (grey, recorded every 5 cycles) and the last one of 50 cycles (red) (2 mM *o*-AP in 0.1 M $HClO_4$ / 0.4 M $NaClO_4$, pH~1); **(c)** Cyclic voltammetry of the final POAP polymer film deposited onto the tip side of the Au-sputtered foil (0.01 M $HClO_4$ / 0.04 M $NaClO_4$, pH~2).

The identity of the polymer film was confirmed by Raman spectroscopy. Results in **Figure 2(a)**, indicates that that the ***c-c'*** couple belongs to a phenoxazine-like chain structure of POAP, in accordance to previously published results.[51,52,54] Compared to the bare PET/Au surface, the region around 1100-1700 cm^{-1} shows the typical bands of arylamine-based polymers.[19,53] More specifically, the outstanding signals associated with POAP are: C-H bending in plane (1170 cm^{-1}), -C-$N^{\cdot+}$ radical semiquinone (1325 cm^{-1}), –C=N- quinoid ring (1475 cm^{-1}) and C=C- aromatic ring (1500 cm^{-1}) stretching vibrations. Also, the spectrum shows the band corresponding to the benzenoid ring deformation at 570 cm^{-1}.[55]

Surface wettability changes were determined by contact angle measurements as shown in **Figure 2(b)**. Several studies have proved the influence of wettability on the ionic transport.[34,56,57] For this reason, the contact angle changes of the Au-coated foil were studied before and after the modification with POAP. Thus, the contact angle values determined with 0.01 M $HClO_4$/0.04 M $NaClO_4$ solution were ~65° and ~30° before and after the polymerization, respectively. The marked increment in the hydrophilicity confirms the functionalization with POAP.

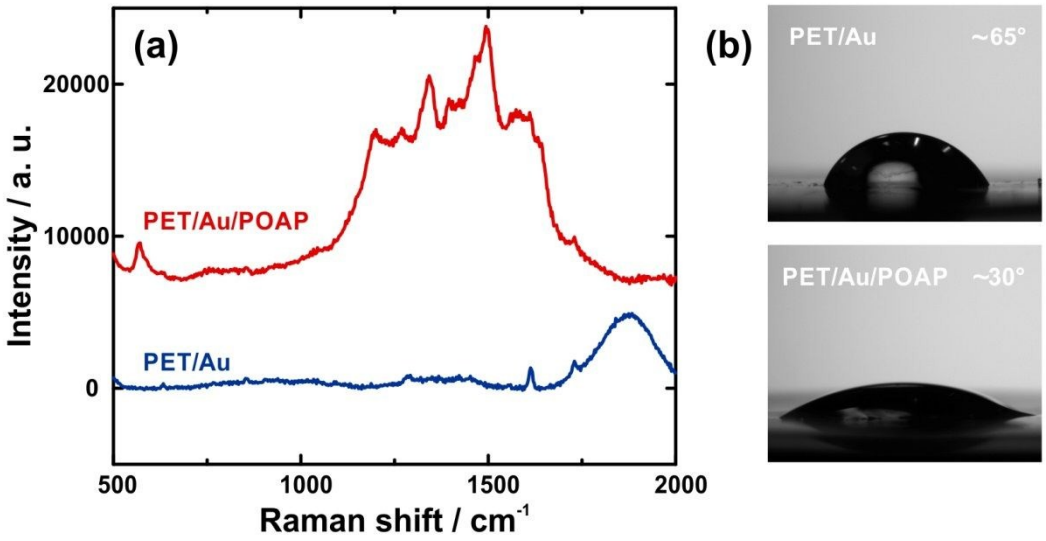

Figure 2. **(a)** Raman spectra of Au-sputtered PET membrane before and after o-AP electropolymerization; **(b)** Contact angle before and after the POAP modification. All measurements were carried out with a 10 mM $HClO_4$ – 40 mM $NaClO_4$ solution.

In order to study the iontronic behavior of the nanochannel, *I-V* curves before and after the electrodeposition of POAP were recorded using a four-electrode arrangement (**Figure S3**). Conductimetric measurements carried out on the Au-coated foil (PET/Au) showed a cation-selective rectified transport, whose selectivity is ascribed to the negative surface charge of the gold layer caused by adsorption of perchlorate ions (**Figure 3, (a)** and **(b)**). As previously reported, rectification effect arises from the disruption of the symmetry in the electric potential along the nanochannels,[13] and perm-selectivity towards a certain type of ion stems from the interaction between mobile ions and surface charged groups in the tip region.[58] Also, the rectification behaviour is highly dependent on factors such as the surface charge, the nanometric size of the nanochannel, the ionic strength, the presence of specific ionic moieties, among others.[4,59–61]

View Article Online
DOI: 10.1039/C9NR10336H

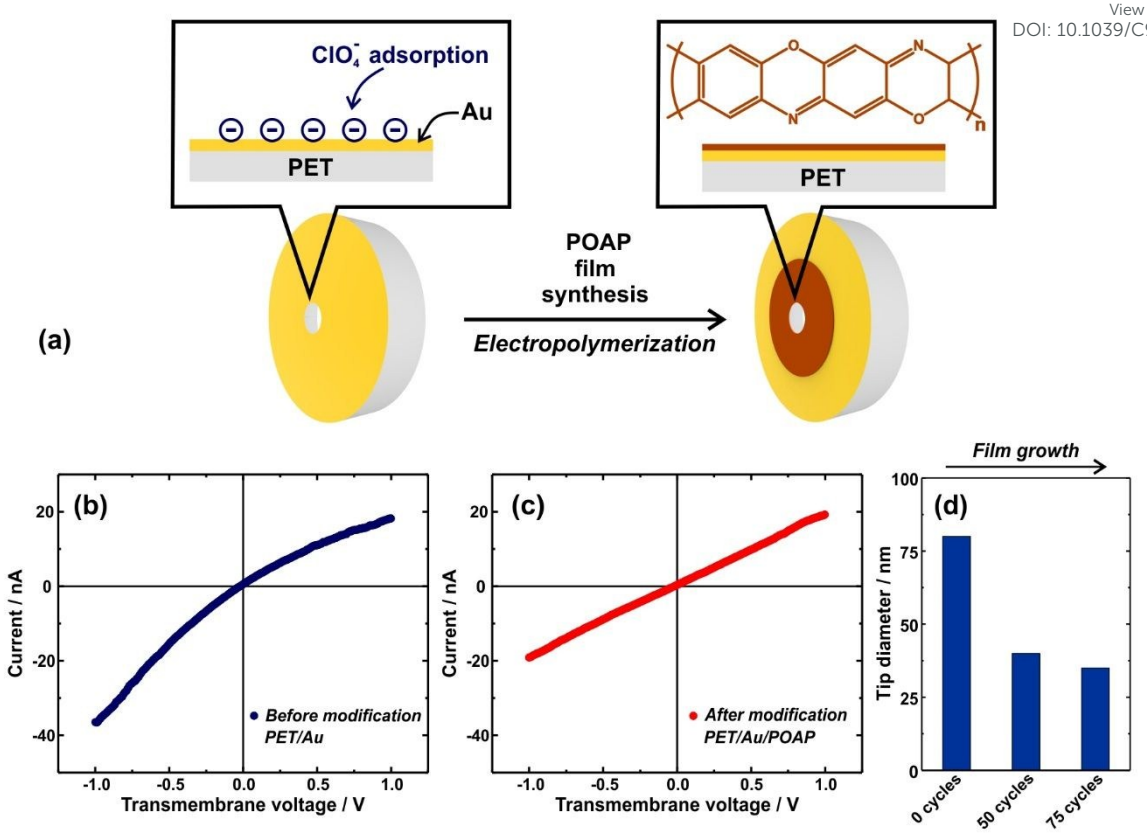

Figure 3. (a) Schematic representation of the electrochemical polymerization of *o*-AP onto the metallized PET membrane containing the bullet-shaped nanopore; *I-V* curves ($HClO_4$ 0.1 M + $NaClO_4$ 0.4 M): (b) before (blue) and (c) after the electropolymerization (red). (d) Tip diameters obtained after different electropolymerization cycles of *o*-AP. The increase in the number of electropolymerization cycles produces an increase in the film thickness with a concomitant decrease in the tip diameter.

After the deposition of POAP, the nanochannel presents a different iontronic response (**Figure 3(b)**). More specifically, after functionalization with POAP, the device showed an ohmic response in high ionic strength acidic conditions. This behaviour suggests that the as-synthesized polymer has a low charge state which, in solutions of high ionic strength, produces the loss of ICR effect. Moreover, a concomitant decrease in transmembrane currents evidences a reduction in the size of d_{tip} after the POAP modification (**Figure 3(d)**). As shown in **Figure 3(d)**, the effective tip diameter estimated from the nanochannel conductance decreases with the number of voltammetric cycles during the electropolymerization of POAP (for further details see SI file). These results are in accordance with previously reported studies on nanochannels modified by other electrochemically active polymers.[21,32] In this regard, electropolymerization on metallized PET nanochannels constitutes a very promising bottom-up strategy to develop rectifying nFETs, due to the precise control on the film thickness and, thus, the possibility of selectively changing the effective tip diameter.

As previously mentioned, POAP is an electroactive polymer formed by phenoxazine units that act as redox centers. Thus, by applying suitable bias voltage, the electroactive polymer can alternate between reduced ($POAP_{(red)}$) and oxidized ($POAP_{(ox)}$) states.[46,51] The reduced state is rich in amine groups whereas the oxidized

state is characterized by the presence of imine groups. The redox behaviour of POAP has been extensively studied by several groups.[55,62–66] In particular, it has been reported that the voltammetric response of POAP films strongly depends on pH. The voltammograms are ill-defined for pH higher than 3 and for pH close to 5 the cathodic peak practically disappears.[53,63] Furthermore, it has been proposed that the redox mechanism in acidic media is complex involves both the addition and elimination of protons.[63] The oxidation of $POAP_{(red)}$ is a two-electron process coupled to the release of two protons. It requires the amine groups in $POAP_{(red)}$ to be protonated and yields non-protonated imine moieties. Thus, the whole process taking place at pH lower than 3 can be depicted as

$$POAP_{(red)}\ (-NH_2^+-) \rightarrow POAP_{(ox)}\ (-N=) + 2e^- + 2\ H^+ \qquad \textbf{(Eq. 1)}$$

The p*Ka* value for the reduced form of POAP has been estimated to be about 2.5.[46,63] Then, at pH lower than 2.5, a high proportion of the amine groups are protonated in $POAP_{(red)}$.[53] On the contrary, the imine groups remain unprotonated even at this highly acidic pH. As a result, the redox conversion of POAP at pH lower than 2.5 implies a net change in the polymer ionic charge from positive in the reduced state to nearly neutral in the oxidized form. Taking into account the marked influence of the surface charge on the ionic transport in nanochannels, the integration of POAP onto the tip side of the nanochannel would produce redox responsiveness to the nanofluidic device, allowing the modulation of the iontronic response by the application of suitable redox potential values to the membrane (gate voltages) (**Scheme 1**). Moreover, the use of highly acidic solutions (pH 1-2) would allow guaranteeing both the reversibility of the POAP redox switching and the differential protonation of the reduced and oxidized forms. Nanofluidic devices operating at such highly acidic conditions are rarely reported, so integration of POAP to SSNs may potentially offer new insights for harsh environment gating applications.

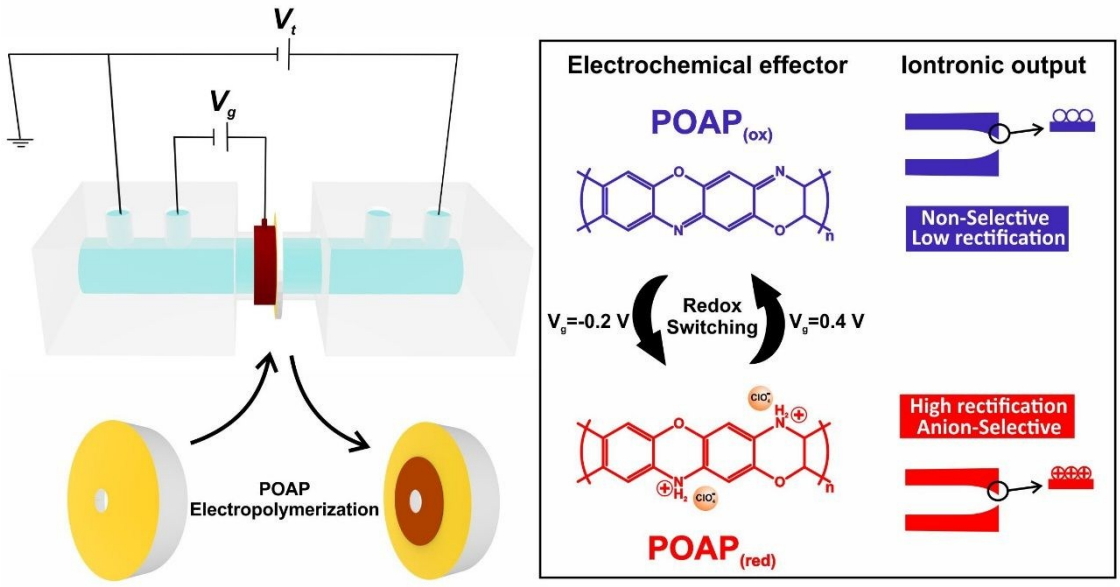

Scheme 1. Scheme of the cell used for POAP nFET measurements (left). The relation between the gate voltage, redox state and the iontronic output for the POAP functionalized nanochannel is presented (right).

In order to control the POAP redox state and to simultaneously record the iontronic output, a bipotentiostat set-up was used (**Figure S3**). Hence, a potentiostat connected in a three-electrode arrangement was used to

control the applied potential to the Au-coated foil, connected to an external Cu ring. This allowed, in a first step, the synthesis of the electroactive polymer film on the tip side by means of the electropolymerization of monomer *o*-AP by cyclic voltammetry. The same three electrode configuration was then employed to control of the POAP redox state through the application of certain potential during the transmembrane measurements. In line with the FET analogy, this potential applied to membrane is also referred to as gate voltage (V_g). Simultaneously, the iontronic response was recorded with another potentiostat set-up connected to a four-electrode array. **Scheme 1** depicts a simplified electrode configuration; further details are presented in the **SI file**.

Figure 4 shows the *I-V* curves recorded at different values of the redox potential applied to the membrane. In agreement with the voltammetric response, the iontronic output showed an appreciable influence of V_g for values around 0.2 V (**Figure 4(a)**). For $V_g > 0.2$ V, the *I-V* curves show a *quasi*-ohmic behaviour, *i.e.* a low ICR ascribed to the low charge state of $POAP_{(ox)}$. However, for $V_g < 0.2$ V, an enhancement of anion-driven rectification was triggered caused by the electrochemical reduction of the POAP film. Appropriate control experiments show that the same iontronic behaviour is obtained when PET/Au membranes are submitted to different V_g values, whereas clear gating effects are obtained after depositing the POAP layer on the same membrane, supporting the idea that V_g causes a change in the iontronic response due to the presence of the POAP film (**Figure S4**).

The ICR mechanism has been explained using different models.[14,67–69] PNP simulations have revealed that the surface charge produces accumulation or depletion of ions in the tip region depending on the applied transmembrane voltage, V_t.[58,67] Particularly in the present system, when V_g is fixed at a value lower than 0.2 V, POAP acquires positive charge due to the reduction of imine groups to charged amine groups. This increment in the surface charge in the nanochannel tip region triggers an enhancement of the ionic rectification. Therefore, the behavior of iontronic output implies that the system can be switched from low-rectifying to anion-driven rectification) by means of the application of very low gate voltages ($-0.2\ V < V_g < 0.2\ V$). Moreover, it is important to emphasize that the system showed good stability in the current measurements (**Figure S5**).

With the aim of quantifying the ICR efficiency of the iontronic response, the rectification factor (f_{rec}) was used. This parameter is calculated as a ratio between the currents at ±1V (see Experimental Section). Previously reported works have demonstrated that f_{rec} is very sensitive to changes in the surface charge as well as in ionic strength, channel diameter and geometry, among others.[4,70–74] Nevertheless, taking into account the experimental conditions used in this work, we are able to ascribe changes in f_{rec} to changes in the POAP surface charge. **Figure 4 (b)** shows the influence of V_g on the ionic transport in terms of f_{rec}. When $V_g > 0.2$ V, the iontronic output exhibited a low f_{rec}, between 2 and 3. This behaviour must be due to the low charge state of $POAP_{(ox)}$ and can be correlated to a low ionic selectivity.[58] On the other hand, when $V_g < 0.2$ V, f_{rec} increased markedly and became ever larger as V_g decreased, in line with the electrochemical reduction of the $POAP_{(ox)}$

to the protonated $POAP_{(red)}$. The study of the influence of pH on the iontronic response of POAP-modified membranes at V_g=-0.2 V (**Figure S6**), allowed confirming the proposed acid-base behaviour for the reduced form of POAP. The analysis in terms of the f_{rec} gives an affective p*Ka* value of 2.4 for this redox form, which is in excellent agreement with the estimated value from electrochemical results.[46,63,66] Hence, in acidic media, unprotonated imine groups in $POAP_{(ox)}$ are reduced to protonated amine groups in $POAP_{(red)}$ and, therefore, a net number of positively charged sites are produced in the film upon electrochemical reduction.[53,63,75] To evaluate the effect of the presumed hydrophobicity change caused by the gate voltage on the iontronic response, the influence of V_g on the contact angle of drops of 10 mM $HClO_4$ + 40 mM $NaClO_4$ solution on Au/POAP electrodes was investigated. Results presented in the **SI file** show no appreciable variations of the contact angle values when changing V_g between -0.2 and 0.4 V (**Figure S7**). These results suggest that the interaction between the charged surface groups and the mobile ions is the main mechanism implicated in the voltage-gated ionic transport of the PET/Au/POAP nanofluidic system.

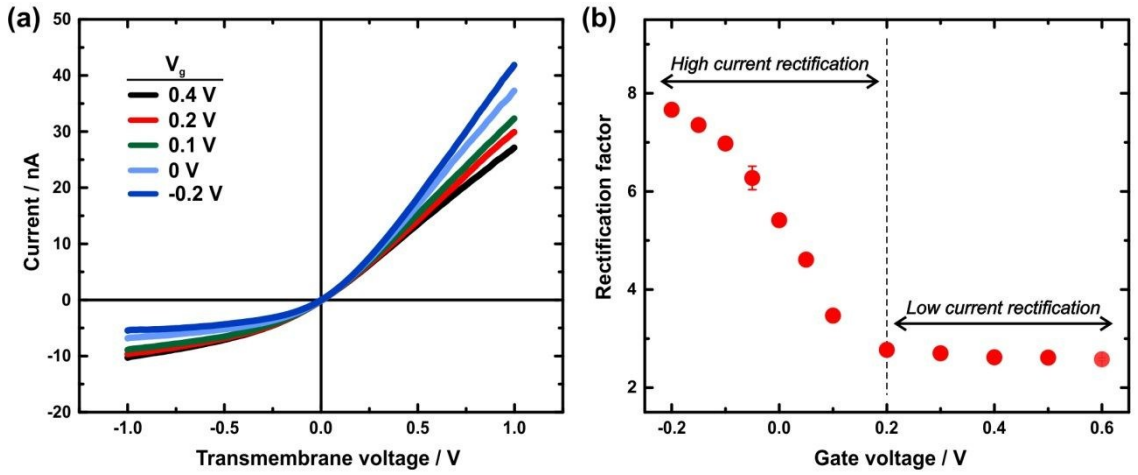

Figure 4. (a) *I-V* curves of the PET/Au/POAP nanochannel at different values of the gate voltage; **(b)** Rectification factors obtained from the *I-V* curves as a function of the gate voltage. All measurements were carried out in a 10 mM $HClO_4$ + 40 mM $NaClO_4$ aqueous solution.

As it arises from results in **Figure 4**, the system displayed a good tuning of ionic transport behavior by the application of low V_g (-0.2 V < V_g < 0.4 V). To test the reversibility of the iontronic response triggered by changes in the redox state of POAP, consecutive experiments switching V_g between -0.2 V and 0.4 V were carried out. These V_g values were selected from the voltammetric response of POAP in this electrolyte solution and the iontronic behavior showed in **Figure 4**, to guarantee the polymer film to be in its reduced (high rectification state) or oxidized form (low rectification state), avoiding the possible interference of any parasite electrochemical reaction (dissolved oxygen reduction or hydrogen evolution) or polymer overoxidation at lower or higher potential limits, respectively. **Figure 5 (a)** shows the switching of the iontronic output in terms of f_{rec}. These changes are related to a reversible transition between the reduced (red circles) and oxidized states (blue circles) of POAP. In agreement with the trend showed in **Figure 4**, the application of a V_g= -0.2V produced the reduction of POAP in the nanochannel tip that caused an increase in the anion-driven rectification. The switching performance in terms of the iontronic current is presented in **Figure 5 (b)** and **(c)**.

Thus, the electrochemical reduction of POAP causes a current increment at V_t = 1 V (high conductance state) and a decrease at V_t = -1 V (low conductance state), which is responsible for a more marked diode-like asymmetry of the iontronic response.

In terms of real-world applications, a fast switching of the iontronic response after changing V_g is desirable. For this reason, the dynamics of the ionic current after V_g perturbations were evaluated (**Figure 6**). For this purpose, we recorded the ionic current at both 1 V and -1 V using a four-electrode array and, simultaneously, a V_g programme employing a three-electrode array was applied. **Figure 6(a)** shows the V_g steps used and **Figure 6 (b)** and **(c)** illustrate the ionic current switching at V_t=1 V and V_t=-1 V, respectively. The zoom-in shows the quick iontronic output dynamics of the nFET. This feature is desirable for the rational design and development of nanochannels with a V_g-modulated selectivity.

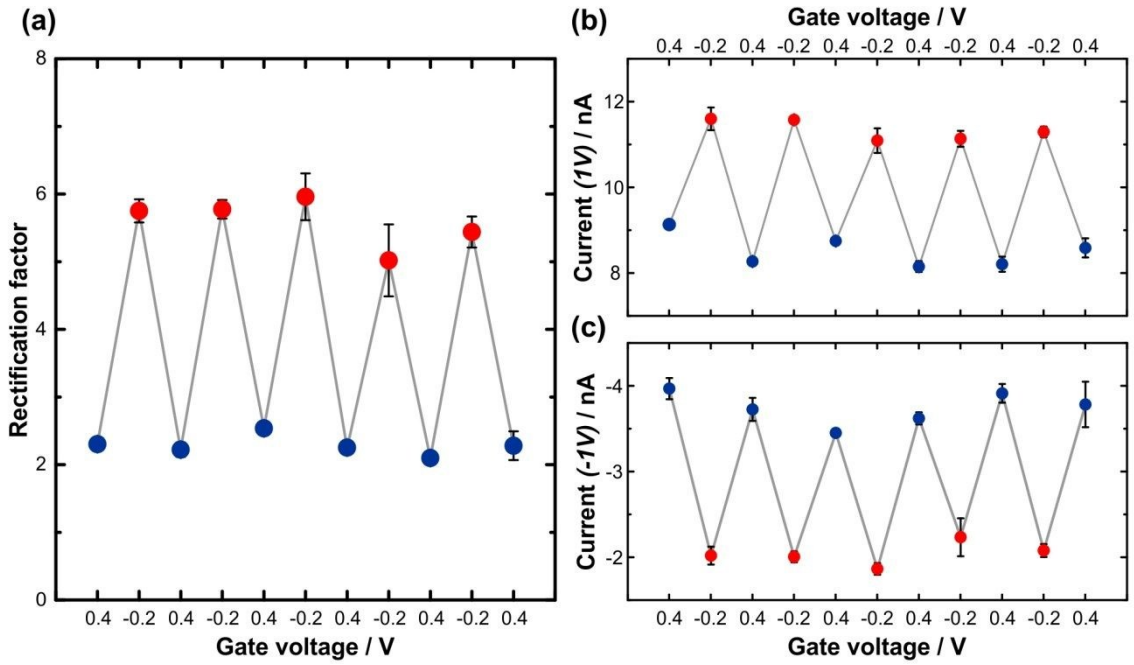

Figure 5. Reversibility tests in terms of: (a) rectification factor, (b) current at V_t= +1V and (c) current at V_t= -1 V. All measurements were carried out in a 10 mM $HClO_4$ + 40 mM $NaClO_4$ solution.

View Article Online
DOI: 10.1039/C9NR10336H

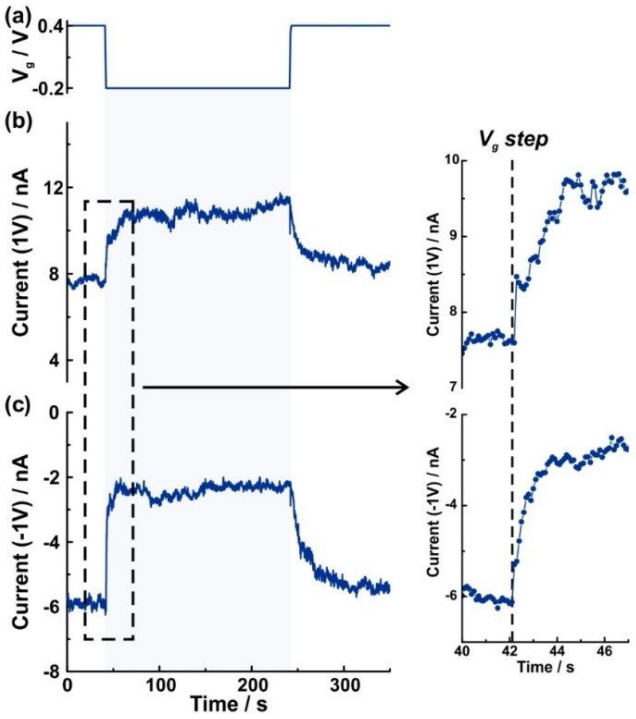

Figure 6. Left panel: (a) Gate voltage program used to study the dynamics of the device. Variations in the transmembrane current at (b) V_t = +1 V and (c) V_t = -1 V; Right panel: zoom-in of the transition region. All measurements were carried out in a 10 mM $HClO_4$ + 40 mM $NaClO_4$ solution. Figure (b) and (c) were obtained in different experiments with the same nanochannel and V_g programme.

Conclusions

In summary, a nanofluidic field-effect transistor (nFET) based on the integration of the electroactive polymer POAP to SSNs was presented. This device allowed the precise control of ionic transport via the handling of a non-invasive stimulus as it is the gate voltage, V_g. Firstly; the tip of a bullet-shaped PET nanochannel fabricated by ion-track-etching was coated with Au and subsequently modified with POAP by electropolymerization. An interesting feature of the modification method is that it allows a fine control on the final tip diameter by managing the number of electropolymerization cycles. Furthermore, the application of different bias potentials V_g to the polymer film enabled the control of the POAP redox state and, consequently, the nanochannel surface charge. More specifically, precise control in the iontronic output by means of the application of low V_g (<|0.2| V) was achieved. In this regard, the present system exhibited good reversibility with a quick and reliable response to the switching of V_g.

This work is a new example of the high potential of nFETs based on the integration of electroactive polymers to nanofluidic devices. The versatility of electroactive polymers added to the fascinating properties of SSNs can be a simple way for facing up the development of devices with applications in fields such as filtration and nanoelectronics. Nanofluidic field-effect transistors constitute an emerging field and further studies are necessary to explore their potentialities and definite applications.

Experimental Section

Materials. Monomer *o*-amino-phenol (*o*-AP) was purchased from Fluka. Perchloric acid and sodium hydroxide were of analytical grade. All reagents were used without further purification.

Etching Procedure. 12 μm-thick PET foils were irradiated with a single swift heavy ion (~2 GeV Au) at the UNILAC linear accelerator of GSI Helmholtzzentrum für Schwerionenforschung. The damage induced to the material along the ion trajectory was removed by selective chemical etching, thus converting the ion track in a bullet-shaped nanochannel.[50] The etching procedure was performed in a home-made cell where one compartment was filled with 6 M NaOH at 60 °C for 7-8 min while the other side contained 6 M NaOH plus a small amount of anionic surfactant Dowfax 2a1 (0.05%). After etching, membranes were rinsed several times with Milli-Q water (18.2 MΩ·cm at 25 °C) and stored also in water.

Au deposition. A gold thin film (~80 nm) was deposited onto the tip side of PET foils (PET/Au) by sputtering as described previously.[32] The Au layer was used as working electrode for the electropolymerization.

Electrochemical synthesis of POAP. 3 mg of *o*-AP were dissolved in 10 ml of $HClO_4$ 0.1/ $NaClO_4$ 0.4 M solution. POAP polymerization over the PET/Au foil was performed in a home-made conductivity cell (**Figure S3**) by cycling the potential between -0.25 and 0.8 V at a scan rate of 100 mV s^{-1}.

Spectroscopic measurements. Raman spectra were obtained with a BWTek Raman spectrometer (BWS415-532S) equipped with optical microscope (BAC151B model). The excitation wavelength was 532 nm and the laser was focused on the sample using a 20x optical magnification. Laser power was held at 50 mW. Spectra were recorded in the region of 100 to 4000 cm^{-1}.

Conductimetric measurements. A bipotentiostat setup constituted of two potentiostats (*Reference 600, Gamry Instruments*) was used to apply both transmembrane and gate voltages independently. One of the potentiostats was used to measure the current–voltage (iontronic output) curves of the nanochannel (four-electrode configuration) and the other one was simultaneously used to apply different gate voltages using a typical three-electrode configuration. A detailed scheme of the experimental setup used for the field-effect measurements is shown in the supporting information (**Figure S3**).

Acknowlegdements

G.L., V. M. C. and Y.T.T. acknowledge a scholarship from CONICET. M.L.C., W.A.M. and O.A. are CONICET fellows and acknowledge financial support from Universidad Nacional de La Plata (PPID-X016), CONICET (PIP-0370) and ANPCyT (PICT-2017-1523 and PICT2016-1680). C.T. and M.E.T.M. acknowledge support by the LOEWE project iNAPO funded by the Hessen State Ministry of Higher Education, Research and Arts. The irradiated PET foils are part of the experiment UMAT, which was performed at the beam line X0 at the GSI Helmhotzzentrum fuer Schwerionenforschung, Darmstadt (Germany) in the frame of FAIR Phase-0.

References

View Article Online
DOI: 10.1039/C9NR10336H

1 B. Hille, *Ion Channels of Excitable Membranes*, Oxford University Press, 3rd edn., 2001.

2 Z. S. Siwy and S. Howorka, *Chem. Soc. Rev.*, 2010, **39**, 1115–1132.

3 K. Xiao, L. Wen and L. Jiang, *Small*, 2016, **12**, 2810–2831.

4 G. Pérez-Mitta, A. G. Albesa, C. Trautmann, M. E. Toimil-Molares and O. Azzaroni, *Chem. Sci.*, 2017, **8**, 890–913.

5 X. X. Hou, W. Guo and L. Jiang, *Chem. Soc. Rev.*, 2011, **40**, 2385.

6 G. Pérez-Mitta, M. E. Toimil-Molares, C. Trautmann, W. A. Marmisollé and O. Azzaroni, *Adv. Mater.*, 2019, 1901483.

7 R. Spohr, *Ion Tracks and Microtechnology: Principles and Applications*, Vieweg+Teubner Verlag, 1st editio., 1990.

8 X. Hou, H. Zhang and L. Jiang, *Angew. Chemie - Int. Ed.*, 2012, **51**, 5296–5307.

9 I. Vlassiouk, S. Smirnov and Z. Siwyt, *Nano Lett.*, 2008, **8**, 1978–1985.

10 P. Y. Apel, Y. E. Korchev, Z. Siwy, R. Spohr and M. Yoshida, *Nucl. Instruments Methods Phys. Res. Sect. B Beam Interact. with Mater. Atoms*, 2001, **184**, 337–346.

11 B. Schiedt, K. Healy, A. P. Morrison, R. Neumann and Z. Siwy, *Nucl. Instruments Methods Phys. Res. Sect. B Beam Interact. with Mater. Atoms*, 2005, **236**, 109–116.

12 K. Xiao, P. Li, G. Xie, Z. Zhang, L. Wen and L. Jiang, *RSC Adv.*, 2016, **6**, 55064–55070.

13 H. Zhang, X. Hou, J. Hou, L. Zeng, Y. Tian, L. Li and L. Jiang, *Adv. Funct. Mater.*, 2015, **25**, 1102–1110.

14 Z. S. Siwy, *Adv. Funct. Mater.*, 2006, **16**, 735–746.

15 G. Pérez-Mitta, A. S. Peinetti, M. L. Cortez, M. E. Toimil-Molares, C. Trautmann and O. Azzaroni, *Nano Lett.*, 2018, **18**, 3303–3310.

16 B. Niu, K. Xiao, X. Huang, Z. Zhang, X.-Y. Kong, Z. Wang, L. Wen and L. Jiang, *ACS Appl. Mater. Interfaces*, 2018, **10**, 22632–22639.

17 K. Xiao, L. Chen, Z. Zhang, G. Xie, P. Li, X. Y. Kong, L. Wen and L. Jiang, *Angew. Chemie - Int. Ed.*, 2017, **56**, 8168–8172.

18 S. Prakash, H. A. Zambrano, M. Fuest, C. Boone, E. Rosenthal-Kim, N. Vasquez and A. T. Conlisk, *Microfluid. Nanofluidics*, 2015, **19**, 1455–1464.

19 P. Li, G. Xie, X. Y. Kong, Z. Zhang, K. Xiao, L. Wen and L. Jiang, *Angew. Chemie - Int. Ed.*, 2016, **55**, 15637–15641.

20 Y.-B. Zheng, S. Zhao, S.-H. Cao, S.-L. Cai, X.-H. Cai and Y.-Q. Li, *Nanoscale*, 2017, **9**, 433–439.

21 G. Pérez-Mitta, W. A. Marmisolle, L. Burr, M. E. Toimil-Molares, C. Trautmann and O. Azzaroni, *Small*, 2018, **1703144**, 1703144.

22 B. Yameen, M. Ali, R. Neumann, W. Ensinger, W. Knoll and O. Azzaroni, *Small*, 2009, **5**, 1287–1291.

23 S. Prakash and A. T. Conlisk, *Lab Chip*, 2016, **16**, 3855–3865.

24 W. Guan, S. X. Li and M. A. Reed, *Nanotechnology*, 2014, **25**, 122001.

25 C. Cheng, G. Jiang, G. P. Simon, J. Z. Liu and D. Li, *Nat. Nanotechnol.*, 2018, **13**, 685–690.

26 Y. Gogotsi, *Nat. Nanotechnol.*, 2018, **13**, 625–627.

27 K.-G. Zhou, K. S. Vasu, C. T. Cherian, M. Neek-Amal, J. C. Zhang, H. Ghorbanfekr-Kalashami, K. Huang, O. P. Marshall, V. G. Kravets, J. Abraham, Y. Su, A. N. Grigorenko, A. Pratt, A. K. Geim, F. M. Peeters, K. S. Novoselov and R. R. Nair, *Nature*, 2018, **559**, 236–240.

28 Y. Wang, H. Zhang, Y. Kang, Y. Zhu, G. P. Simon and H. Wang, *ACS Nano*, 2019, **13**, 11793–11799.

29 C. R. Martin, M. Nishizawa, K. Jirage, M. Kang and S. B. Lee, *Adv. Mater.*, 2001, **13**, 1351–1362.

30 E. B. Kalman, O. Sudre, I. Vlassiouk and Z. S. Siwy, *Anal. Bioanal. Chem.*, 2009, **394**, 413–419.

31 G. Pérez-Mitta, W. A. Marmisollé, C. Trautmann, M. E. Toimil-Molares and O. Azzaroni, *Adv. Mater.*, 2017, **1700972**, 1–6.

32 G. Pérez-Mitta, W. A. Marmisollé, C. Trautmann, M. E. Toimil-Molares and O. Azzaroni, *J. Am. Chem. Soc.*, 2015, **137**, 15382–15385.

33 G. Laucirica, W. A. Marmisollé, M. E. Toimil-Molares, C. Trautmann and O. Azzaroni, *ACS Appl. Mater. Interfaces*, 2019, **11**, 30001–30009.

34 Q. Zhang, J. Kang, Z. Xie, X. Diao, Z. Liu and J. Zhai, *Adv. Mater.*, 2017, **1703323**, 1–7.

35 Q. Zhang, Z. Zhang, H. Zhou, Z. Xie, L. Wen, Z. Liu, J. Zhai and X. Diao, *Nano Res.*, 2017, **10**, 3715–3725.

36 R. Ren, Y. Zhang, B. P. Nadappuram, B. Akpinar, D. Klenerman, A. P. Ivanov, J. B. Edel and Y. Korchev, *Nat. Commun.*, 2017, **8**, 586.

37 G. Inzelt, *Conducting Polymers: A New Era in Electrochemistry*, Springer-Verlag Berlin Heidelberg, 2008.

38 M. E. G. Lyons, *Electroactive Polymer Electrochemistry*, Springer US, Boston, MA, 1st Editio., 1994.

39 E. M. Geniès, A. Boyle, M. Lapkowski and C. Tsintavis, *Synth. Met.*, 1990, **36**, 139–182.

40 Z. H. Wang, C. Li, E. M. Scherr, A. G. MacDiarmid and A. J. Epstein, *Phys. Rev. Lett.*, 1991, **66**, 1745–1748.

41 C. Dhand, M. Das, M. Datta and B. D. Malhotra, *Biosens. Bioelectron.*, 2011, **26**, 2811–2821.

42 Q. Wu, Y. Xu, Z. Yao, A. Liu and G. Shi, *ACS Nano*, 2010, **4**, 1963–1970.

43 C. Barbero, J. Zerbino, L. Sereno and D. Posadas, *Electrochim. Acta*, 1987, **32**, 693–697.

44 W. A. Marmisollé, D. Gregurec, S. Moya and O. Azzaroni, *ChemElectroChem*, 2015, **2**, 2011–2019.

45 R. Tucceri, *Procedia Mater. Sci.*, 2015, **8**, 261–270.

46 R. Tucceri, *Poly(o-aminophenol) Film Electrodes: Synthesis, Transport Properties and Practical Applications*, Springer International Publishing, 1st Editio., 2013.

47 T. Ohsaka, S. Kunimura and N. Oyama, *Electrochim. Acta*, 1988, **33**, 639–645.

48 A. Guerrieri, R. Ciriello and D. Centonze, *Biosens. Bioelectron.*, 2009, **24**, 1550–1556.

49 W. Tao, D. Pan, Y. Liu, L. Nie and S. Yao, *Anal. Biochem.*, 2005, **338**, 332–340.

50 P. Y. Apel, I. V. Blonskaya, S. N. Dmitriev, O. L. Orelovitch, A. Presz and B. A. Sartowska, *Nanotechnology*, 2007, **18**, 305302.

51 C. Barbero, J. J. Silber and L. Sereno, *J. Electroanal. Chem.*, 1989, **263**, 333–352.

52 H. J. Salavagione, J. Arias, P. Garcés, E. Morallón, C. Barbero and J. L. Vázquez, *J. Electroanal. Chem.*, 2004, **565**, 375–383.

53 R. I. Tucceri, C. Barbero, J. J. Silber, L. Sereno and D. Posadas, *Electrochim. Acta*, 1997, **42**, 919–927.

54 J. M. Ortega, *Thin Solid Films*, 2000, **371**, 28–35.

55 H. J. Salavagione, J. Arias-Pardilla, J. M. Pérez, J. L. Vázquez, E. Morallón, M. C. Miras and C. Barbero, *J. Electroanal. Chem.*, 2005, **576**, 139–145.

56 G. Xie, P. Li, Z. Zhao, Z. Zhu, X.-Y. Y. Kong, Z. Zhang, K. Xiao, L. Wen and L. Jiang, *J. Am. Chem. Soc.*, 2018, **140**, 4552–4559.

57 M. R. Powell, L. Cleary, M. Davenport, K. J. Shea and Z. S. Siwy, *Nat. Nanotechnol.*, 2011, **6**, 798–802.

58 J. Cervera, B. Schiedt, R. Neumann, S. Mafá and P. Ramírez, *J. Chem. Phys.*, 2006, **124**.

59 C. Wei, A. J. Bard and S. W. Feldberg, *Anal. Chem.*, 1997, **69**, 4627–4633.

60 Z. Siwy, E. Heins, C. C. Harrell, P. Kohli and C. R. Martin, *J. Am. Chem. Soc.*, 2004, **126**, 10850–10851.

61 G. Laucirica, G. Pérez-Mitta, M. E. Toimil-Molares, C. Trautmann, W. A. Marmisollé and O. Azzaroni, *J. Phys. Chem. C*, 2019, **123**, 28997–29007.

62 Z. You-Yu, W. Mei-Ling, L. Mei-Ling, Y. Qin, X. Qing-Ji and Y. Shou-Zhuo, *Chinese J. Anal. Chem.*, 2007, **35**, 685–690.

63 M. E. Carbone, R. Ciriello, S. Granafei, A. Guerrieri and A. M. Salvi, *Electrochim. Acta*, 2015, **176**, 926–940.

64 T. Komura, Y. Ito and K. Takahasi, *Electrochim. Acta*, 1998, **43**, 723.

65 S. Kunimura, T. Ohsaka and N. Oyama, *Macromolecules*, 1988, **21**, 894–900.

66 C. Barbero, J. J. Silber and L. Sereno, *J. Electroanal. Chem. Interfacial Electrochem.*, 1990, **291**, 81–101.

67 J. Wang, M. Zhang, J. Zhai and L. Jiang, *Phys. Chem. Chem. Phys.*, 2014, **16**, 23–32.

68 Z. Siwy and A. Fuliński, *Phys. Rev. Lett.*, 2002, **89**, 4–7.

69 A. Fuliński, I. Kosińska and Z. Siwy, *New J. Phys.*, 2005, **7**, 132.

70 P. Y. Apel, I. V. Blonskaya, O. L. Orelovitch, P. Ramirez and B. A. Sartowska, *Nanotechnology*, 2011, **22**, 1–13.

71 P. Ramírez, P. Y. Apel, J. Cervera and S. Mafé, *Nanotechnology*, 2008, **19**, 315707.

72 G. Pérez-Mitta, A. Albesa, F. M. Gilles, M. E. Toimil-Molares, C. Trautmann and O. Azzaroni, *J. Phys. Chem. C*, 2017, **121**, 9070–9076.

73 Z. Zhang, L. Wen and L. Jiang, *Chem. Soc. Rev.*, 2018, **47**, 322–356.

74 M. Ali, B. Yameen, J. Cervera, P. Ramírez, R. Neumann, W. Ensinger, W. Knoll, O. Azzaroni, P. Ramı, R. Neumann, W. Ensinger, W. Knoll and O. Azzaroni, *J. Am. Chem. Soc.*, 2010, **132**, 8338–8348.

75 R. I. Tucceri, *J. Electroanal. Chem.*, 2003, **543**, 61–71.

View Article Online
DOI: 10.1039/C9NR10336H

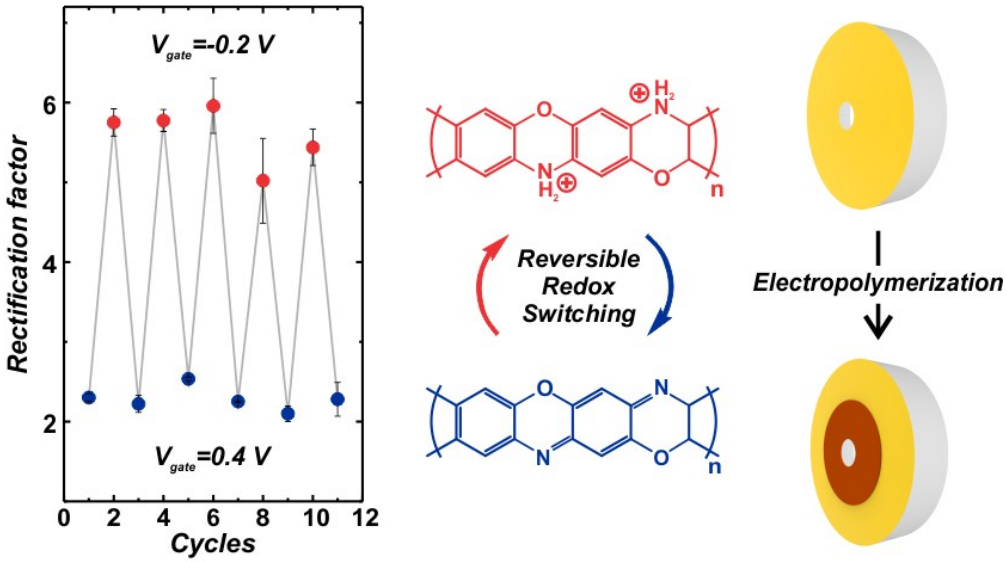

ToC Graphic